Single Crystal Gallium Nitride Nanomembrane Photoconductor and Field Effect Transistor

*Kanglin Xiong, Sung Hyun Park, Jie Song, Ge Yuan, Danti Chen, Benjamin Leung, and Jung Han**

Large-area, free-standing and single-crystalline GaN nanomembranes are prepared by electrochemical etching from epitaxial layers. As-prepared nanomembranes are highly resistive but can become electronically active upon optical excitation, with an excellent electron mobility. The interaction of excited carriers with surface states is investigated by intensity-dependent photoconductivity gain and temperature-dependent photocurrent decay. Normally off enhancement-type GaN nanomembrane MOS transistors are demonstrated, suggesting that GaN could be used in flexible electronics for high power and high frequency applications.

1. Introduction

Single crystal semiconductor nanomembranes have attracted much attention due to their unique electronic, optoelectronic, and mechanical properties, as well as the potential for heterogeneous integration.[1–4] Silicon nanomembranes have been prepared by undercut etching of SOI structures. GaAs (InAs) membranes released by AlAs (AlGaSb) undercut layers have been demonstrated to be promising for photonic[2] and electronic[4] applications. Wide bandgap GaN is one of the most important electronic materials. Dislocation-free GaN membrane has been exfoliated with limited lateral dimension.[5] There have also been efforts and demonstrations in separating μm-thick GaN device structures from substrates using laser liftoff,[6] chemical liftoff,[7] electrochemical liftoff,[8,9] and mechanical liftoff on suitable buffer layers.[10,11] These works open the way for vertical device configuration but fall short in the pursuit of ultrathin (<500 nm), mechanically flexural membranes. As the freestanding layer thickness decreases to below 500 or even 100 nm, the flexural rigidity of the layer is expected to decrease dramatically.[1] At the same time, the active region within a nanomembrane could couple electronically with the surrounding surfaces, bringing both challenges and opportunities.[3] However, these properties are rarely studied for GaN due to the lack of thin, large-area and high quality GaN membrane.

K. Xiong, S. H. Park, J. Song, G. Yuan, D. Chen, B. Leung, J. Han
Department of Electrical Engineering
Yale University
New Haven, CT 06520, USA
E-mail: jung.han@yale.edu

DOI: 10.1002/adfm.201401438

We report in this work the fabrication of single crystal GaN nanomembranes, with a thickness as low as 50 nm. Large area (≥5 mm × 5 mm) GaN membranes are produced by electrochemical etching (ECE) with a special high-conductivity sacrificial underlayer. Large-area, crack-free transfer of GaN NMs have been performed onto metal, glass, and polymer target substrates. The transport properties of freestanding GaN nanomembranes are analyzed using UV-assisted Hall measurements. The interaction of the carriers with the surface electronic states are investigated by the intensity dependence of the photoconductor gain, and by the temperature-dependent measurements of photocurrent decay. The transport property of GaN NM, down to a thickness of 90 nm, remains very comparable to that from much thicker GaN structures. Enhancement-mode field effect transistors (FETs) have been fabricated and demonstrated on a SiO_2/Si(001) wafer, suggesting that GaN nanomembranes can be a new candidate for flexible electronics requiring high power and high-frequency.

2. Results and Discussion

2.1. Nanomembrane Fabrication

The principle of using an ECE process to selectively remove underlying GaN sacrificial layers has been described before.[12,13] Multi-layered GaN structures having nanomembrane layers (50 to 500 nm thick) on top of heavily-doped ($n \approx 1 \times 10^{19}$ cm^{-3}) GaN sacrificial layers were grown by metal-organic chemical vapor deposition (MOCVD) process on sapphire. To obtain large-area NM within a reasonable time, a periodic array of via holes were created such that the undercut etching can proceeds uniformly around these openings. The via-holes are squares with a dimension of 10 μm and a diagonal periodicity of 25, 50, and 100 μm. These holes were created by Cl-based inductively coupled plasma (ICP) etching to expose the sacrificial layer. The photoresist (Shipley S1827) used during the Cl-ICP etching was retained to protect the front surface of the membrane during ECE. The nanomembrane layers became detached from the substrate once the undercut regions around each opening coalesce with the adjacent ones. GaN NMs were cleaned by rinsing sequentially in DI water, acetone and isopropyl-alcohol (IPA). After cleaning, they were transferred on to other substrates

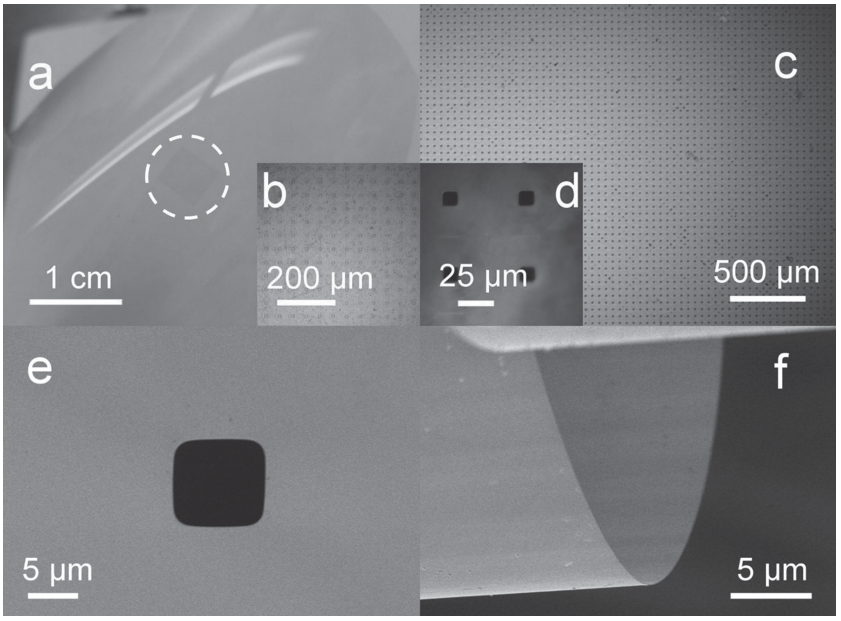

Figure 1. Images of 90 nm thick GaN membranes, with scale bars from 1 centimeter down to 3 micrometer. a) Photo of GaN membrane on PET film, optical microscopy image of b) membrane on PET, c) on SiO2, and d) freestanding membrane. SEM image of e) Ga-polar surface of a freestanding membrane, the black square is hole for electrochemical etching, the light gray area is membrane. f) Membrane under strain to form a curved structure.

by wet transfer methods.[14] In this work the choice of target substrates includes sapphire, silicon and polyethylene terephthalate (PET) films.

Figure 1(a) shows a photograph of 5 mm × 5 mm 90 nm GaN nanomembrane transferred onto a PET film. The inset (b) is a 200× optical microscopy image of the membrane, which is conformal to the PET film. The grid-like pattern is due to the periodic etching vias described earlier. Figure 1(c) is optical microscopy of another 90 nm GaN membrane transferred onto a SiO_2/Si(001) substrate. The inset (d) is a 1000× optical microscopy image of a freestanding membrane. A scanning electron microscopy (SEM) image of the front surface ((0001), Ga-polar) of GaN NM is shown in Figure 1(e), indicating that the surface is generally flat and featureless. Atomic force microscopy (AFM) measurement on the Ga-polar surface of NM reveals (not shown) that the surface retains the step flow morphology of epitaxial GaN. Figure 1(f) shows a 90 nm thick GaN membrane under strain introduced during transfer onto a metal grid to form a curved structure, having a radius of curvature of only 15 μm. This demonstration of a much reduced flexural rigidity suggests that GaN NMs could extend the functionality of III-nitride devices into piezotronics and piezophotonics.[15]

2.2. X-ray Diffraction

High resolution X-ray diffraction was performed to examine the crystal quality of the transferred NMs. **Figure 2**(a) shows the (002) triple-crystal ω-2θ scan of a membrane transferred onto a silicon substrate. The single peak (around 17.16°) confirms the single crystallinity. The presence of fringe peaks on both sides, which are due to x-ray interference, indicates that the top and bottom surfaces of the GaN NM are smooth. The spacing of the fringes gives an estimate of the thickness of the membrane to be 85 nm, in good agreement with the growth design and the SEM measurement. (002) and (102) X-ray rocking curves are shown in Figure 2(b) and 2(c), where the data from the 2.36 μm thick as-grown sample on sapphire (black dashed lines) are juxtaposed with the membrane data (in red). The beam size for the scans is 0.1 mm × 20 mm. The off-axis (102) curve was measured in skew-symmetric geometry. In Figure 2(a), the (002) FWHM is 0.172 degree for membrane, compared to 0.089 degree for the as-grown sample. Such broadening has been observed in Si nanomembrane.[16] It is likely due to the extreme thickness of the NM. From Scherrer's equation ($\Delta\omega = \lambda/d\cos\theta$), the broadening with a 95-nm membrane would be around 0.09°. The (102) diffraction for the NM has a FWHM of 0.135°; in this case the broadening is less (≈0.02°) due to larger thickness seen by X-ray.

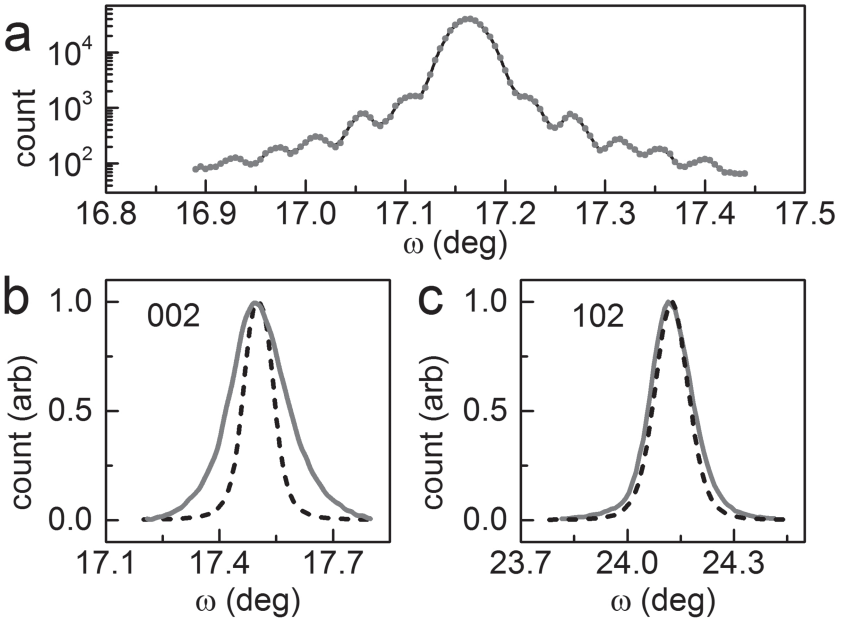

Figure 2. High resolution X-ray diffraction measurement of GaN nanomembrane transferred onto silicon. a) (002) triple-crystal ω/2-theta scan. b) (002) and c) (102) rocking curves of GaN membrane (solid line) and as grown sample (black dot).

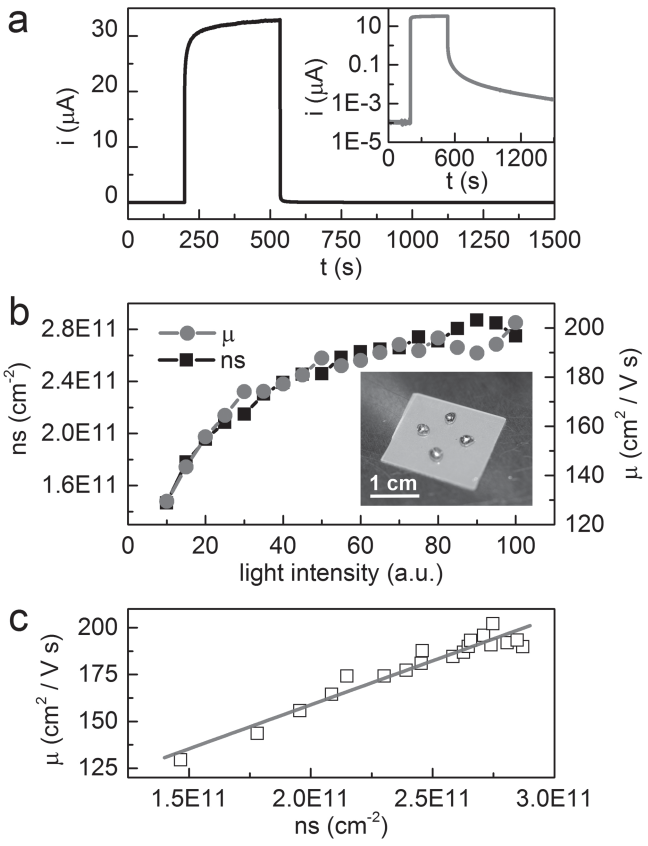

Figure 3. a) Current–time (*i*–*t*) characteritics of 90 nm GaN membrane bias at two adjacent corners with 20 V. UV light was turned on at 200 s and off at about 500 s. The inset shows log(*i*)–*t*. b) Electron concentration and mobility in 90 nm membrane measured under different UV light intensity. The inset is the Hall device on sapphire under test. c) Electron mobility vs. concentration. The line is for eyes only.

2.3. UV-assisted Hall Measurement

Given the innate couplings to surfaces and surroundings, the electronic and optoelectronic properties of GaN NMs are of particular interest in our investigation. As a reference, unintentionally doped (UID) GaN on sapphire prepared by MOCVD exhibits a lightly n-type background concentration of about 5×10^{16} cm^{-3} with a mobility of 600 cm^2 V^{-1} s^{-1}.[17] The sheet resistance of a 90-nm thick GaN NM is estimated to be around 20 KΩ if the NM has the identical transport property. However, all the 140 nm-thick and thinner membranes on either SiO_2/Si or sapphire prepared in our lab are found to be highly resistive by Van der Pauw method. **Figure 3**(a) shows the current-time (*i*-*t*) characteristics measured between two corner contacts from a nanomembrane (90 nm thick, 5×5 mm^2) on sapphire with a 20 V bias. With a dark current level below the nA range, it is challenging to have accurate Hall measurement. The conductivity is drastically improved, in contrast, when the edge area of membrane under the same steady bias is subject to the excitation of a UV (325 nm He-Cd laser) illumination with a power density of 70 mW cm^{-2}. With photo-generated carriers, Hall measurement could be carried out, and by changing the light intensity, carrier concentration could be adjusted.

An UV LED ($\lambda = 365$ nm, $\Delta\lambda = 10$ nm) was used as the excitation source with a tunable optical power. The power density is about 0.9 mW/cm^2 at 50 mA, and is approximately linear to current. A magnet of 0.5 T was used for Hall measurement. For both van der Pauw and Hall measurement, the current bias was 10 μA. A picture of the GaN NM (90 nm) on sapphire under test with gallium droplets as ohmic contacts on the four corners is shown in the inset of Figure 3(b). The sample was prepared by ECE, DI water, acetone and IPA cleaning, transferring the NM onto sapphire, and making ohmic contacts. No further treatment is applied. The top surface of NM is in contact with air while to bottom with sapphire. During the measurements, the NM is regarded as continuous. And electrons are considered as major carriers because of much lower hole than electron mobility in n-type GaN.[18] Influence of holes and patterned holes on the measurements are described in the Supporting Information. Figure 3(b) summarizes the measured sheet carrier density (black squares) and mobilities (red dots) as a function of excitation power. The sheet carrier density increases with light intensity but gradually saturates at higher excitation. The mobility follows a similar trend. Plotting mobility and carrier concentration together in Figure 3(c), we find that the mobility increases linearly with the carrier concentration. It was reported that at low carrier density, an increase in free carriers tends to screen out the scattering due to charged dislocations, which in return enhances the electron mobility.[19] The average electron density here is estimated (assuming a 90-nm thickness) to be $1–3 \times 10^{16}$ cm^{-3}, in agreement with the previously reported results. The measured mobility in the range of 100–200 cm^2 V^{-1} s^{-1} was lower than that from GaN epilayers on sapphire, most likely due to the additional scattering by surface states in the nanomembranes. We note a similar decrease of electron mobility in silicon nanomembrane.[20]

2.4. Photoconductance and Surface Barrier

Pinning of surface Fermi level due to polarization-related surface states is well known for GaN.[21] It introduces band bending near the surface region, which has a fundamental influence on the carrier distribution and transport in GaN nanostructures. **Figure 4**(a) illustrates the band profiles (E_C and E_V) across a NM assuming a symmetric band bending on both surfaces. The electron potential is higher on both surfaces. If the membrane is thin enough, the adjoining of two surface depletion regions causes the membrane to be full depleted. We note that GaN nanowires were found to be fully depleted by the surface barrier when the diameter is smaller than a certain critical value (80–100 nm).[22] Under optical excitation, the surface bending will cause separation of photo-generated carriers with electrons confined within a thin channel near the center while holes will be forced to a triangular well near the surfaces. The electrons have to overcome the surface barrier by the thermionic emission process to recombine with holes, often causing long decays in photocurrent transient, as shown in the inset of Figure 3(a). Under such a band-bending related charge separation, photocurrent transient typically exhibits a strong dependence on the excitation intensity and temperature.[23]

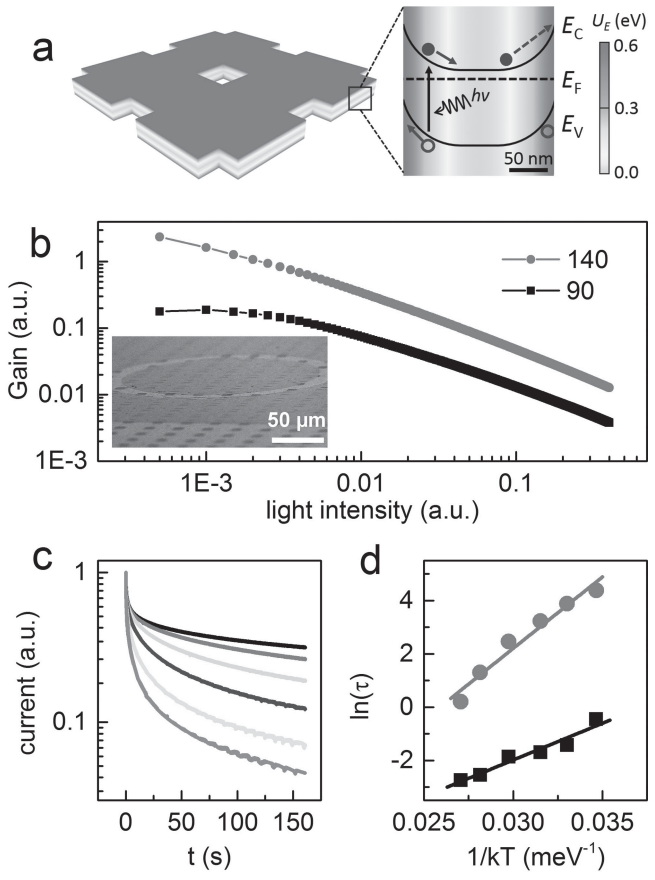

Figure 4. a) Schematic electrical potential distribution (3D color contour) and band diagram within GaN membrane caused by surface Fermi level pinning. b) A log–log plot of the power dependent photocurrent gain for two membrane samples having a thickness of 90 and 140 nm. The inset is a typical circular photoconductor. c) Photocurrent decay of 140 nm membrane measured at 30, 45, 60, 80, 100 and 115 °C, in the order of from top to bottom d) Arrhenius plot of time constants of decay of 90 and 140 nm membrane.

To verify this model, photocurrent has been measured as a function of excitation light intensity. A GaN NM photoconductor device fabricated on SiO_2/Si wafer is shown as the inset of Figure 4(b). The inner circular Ti/Al contact is surrounded by an outer Ti/Al contact with a ring-shaped spacing of 14 μm, both contacts appear as dark regions in this picture. The gain of photocurrent, here defined as current-to-light intensity ratio, is plotted against the light intensity in a log-log plot (Figure 4(b)). Linear fitting of the curves give the slope of –0.91 and –0.85 for membranes with a thickness of 140 nm and 90 nm, respectively. These values suggest that the photocurrent effect is dominated by surface band bending instead of bulk trap effects which should have a value of –0.5.[24]

To quantify the height of the surface barrier, the temperature dependence of photocurrent decay was examined. Since the photocurrent persists for a relatively long time at room temperature, a temperature range of 30 to 120 °C was chosen to investigate the decay transient. The illumination intensity was maintained at a low level (<0.05 mW cm^{-2}) to minimize any modification of band bending due to screening by free carriers.[25] Figure 4(c) shows the result of *i-t* measurement for a 140 nm membrane with increasing temperature. Fitting the curves with stretched exponential function,[24] the temperature-dependent time constants were extracted and are plotted in Figure 4(d) in Arrhenius form. Barrier heights were extracted to be 0.535 eV and 0.275 eV for membranes with a thickness of 140 and 90 nm, respectively. The barrier height for the 140 nm membrane agrees with previously reported values for GaN epilayer and thick nanowire, where surface potential (E_C–E_F) is between 0.5 and 0.6 eV.[21,22] The apparent reduction in barrier height for the 90-nm NM might be due to the thickness effect.[22] Assuming a background impurity level of 1×10^{17} cm^{-3}, the depletion region width is 143 nm and 104 nm for the two barrier heights. This result explains the observed resistivity of membranes in dark. The surface barrier can also explain carrier concentration saturation in Figure 3(b). As the carrier concentration increases with light intensity, the surface barrier will be decreased by free carriers. As a result, the recombination rate will increase, which in turn limits carrier density. It has been noted that GaN nanowire surface barrier heights depend on the surface condition and ambient,[26] the same conclusion may apply to GaN membrane here.

2.5. Field Effect Transistor

To validate its usefulness in electronic applications, GaN NM field effect transistors were fabricated on a SiO_2/n-Si(001) substrate. A 140 nm GaN NM was transferred onto the SiO2 surface with the Ga-polar surface facing downward. **Figure 5**a shows schematic diagram of a back-gate transistor with GaN membrane as active layer. The inset is a optical microscopy image of a real transistor. The width of the channel is 300 μm. The spacing of holes on membrane is 25 μm in diagonal direction. A layer of 250 nm SiO_2 is used as a dielectric layer for back-gating. Ti/Al/Ni/Au is deposited as an ohmic contact without annealing.[27] All the FETs have been treated with O_2 plasma to reduce surface state effects.[28]

Due to the thick dielectric layer (250 nm), the FET has relatively high gate voltage. Figure 5(b) shows the *I–V* curves measured by sweeping back-gate bias voltage from 20 V to 50 V, with step of 5 V. The upmost one is biased at 50 V. The devices show typical current saturation with knee voltage at about 5 V.

The I_G–V_G of the same device is measured with drain bias of 10 V, shown in Figure 5(c). The ON-OFF current ratio is about 10^5. Maximum g_m derived from Figure 5(c) is 0.55 mS mm^{-1} (0.167 mA/V), and the maximum drain current density is 12 mA/mm. While the fabrication process remains preliminary at present, we note that the performance of this nanomembrane GaN MOSFET is in the same range as those from traditional GaN/sapphire structures,[29] and compared favorably with many other inorganic flexible thin film transistors.[30]

Electron mobility can be extracted from trans-conductance g_m using the following equation

$$\mu = g_m \frac{L^2}{CV_{DS}} \quad (1)$$

The channel length L is 14.5 μm. Using a planar capacitor model with a relative dielectric constant of 3.9 for SiO_2, the gate

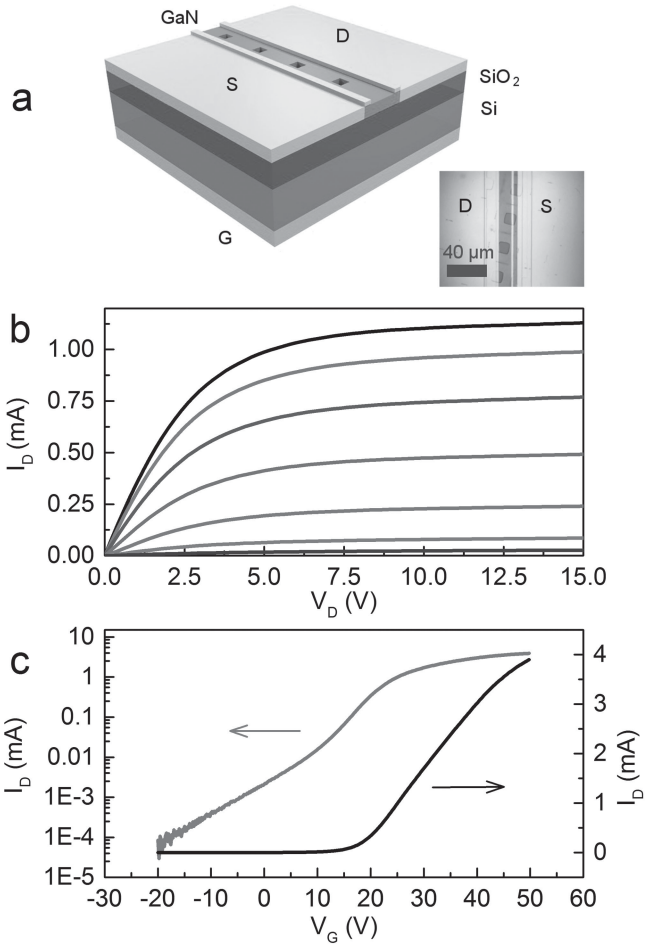

Figure 5. a) Schematic structure of back-gate FET made of GaN membrane. The inset is a optical microscopy image of a 140 nm thick membrane FET. b) Drain current I_D–V_D measured under gate bias from 20 to 50 V, with step of 5 V, in the order of from bottom to top. c) I_D–V_G measure with bias of 10 V.

capacitance C is estimated to be 0.6 pF. Though the bias V_{DS} is 10 V, we can still use knee voltage of 5 V because of current saturation, which yields the mobility of 117 $cm^2\ V^{-1}\ s^{-1}$. From a faster I_G–V_D scan, we also get g_m of 0.22 mA V^{-1}, which corresponds to a mobility of 154 $cm^2\ V^{-1}\ s^{-1}$. These values are slightly lower than Hall measurement. However, they are reasonable, taking surface effects, contact resistance and the etching holes into consideration.

Shift of threshold voltage was observed during measurement. This is due to memory effect of gate which is also found in GaN nanowire FET with "gating hysteresis".[31,32] In the early stage of GaN HEMT devices, researches attributed similar current instability to the trapped charges which serves as a secondary "virtual gate".[33] The traps here could be in the gate oxide SiO_2, at the SiO_2/Si or GaN membrane/SiO_2 interfaces. The nature of these traps is the subject of further study. For the same reason, the current shown in Figure 5(b) is smaller than in Figure 5(c) under the same bias. Because the traps will build up or discharge dynamically, a higher saturated current is observed when the measurement is performed at higher speed.

3. Conclusion

In summary, we have prepared large-area GaN nanomembranes and succeeded in transferring them onto different substrates. The NMs are flexural yet single crystalline, elastic deformation to a radius of curvature of 10 μm is observed without fracture. The NMs are found to be depleted of carriers due to band bending from top and bottom surfaces. UV-assisted Hall measurement has been carried out to ascertain the transport properties; a mobility of 200 $cm^2\ V^{-1}\ s^{-1}$ for a 90 nm membrane indicates its great potential for flexible electronics. The amount of surface band bending and the position of surface Fermi levels are determined by temperature dependent photocurrent decay. Large-area GaN NMs are processed into back-gated, normally off GaN MOS transistors. An ON-OFF ratio of 10^5 has been observed together with very competitive properties for transconductance and maximum drain current. The results here indicate that GaN nanomembrane have a great potential for a variety of applications, such as flexible electronics, sensors, and integration with other semiconductors.

Supporting Information

Supporting Information is available from the Wiley Online Library or from the author.

Acknowledgements

This research was supported by National science foundation (NSF) under Award No. CMMI-1129964, and facilities use were supported by YINQE and NSF MRSEC DMR 1119826.

Received: May 3, 2014
Revised: June 13, 2014
Published online: August 22, 2014

[1] J. A. Rogers, M. G. Lagally, R. G. Nuzzo, *Nature* **2011**, *477*, 45.
[2] J. Yoon, S. Jo, I. S. Chun, I. Jung, H.-S. Kim, M. Meitl, E. Menard, X. Li, J. J. Coleman, U. Paik, J. A. Rogers, *Nature* **2010**, *465*, 329.
[3] P. Zhang, E. Tevaarwerk, B.-N. Park, D. E. Savage, G. K. Celler, I. Knezevic, P. G. Evans, M. A. Eriksson, M. G. Lagally, *Nature* **2006**, *439*, 703.
[4] H. Ko, K. Takei, R. Kapadia, S. Chuang, H. Fang, P. W. Leu, K. Ganapathi, E. Plis, H. S. Kim, S.-Y. Chen, M. Madsen, A. C. Ford, Y.-L. Chueh, S. Krishna, S. Salahuddin, A. Javey, *Nature* **2010**, *468*, 286.
[5] R. T. ElAfandy, M. A. Majid, T. K. Ng, L. Zhao, D. Cha, B. S. Ooi, *Adv. Funct. Mater.* **2013**, *24*, 2305.
[6] W. S. Wong, T. Sands, N. W. Cheung, M. Kneissl, D. P. Bour, P. Mei, L. T. Romano, N. M. Johnson, *Appl. Phys. Lett.* **1999**, *75*, 1360.
[7] K. J. Lee, J. Lee, H. Hwang, Z. J. Reitmeier, R. F. Davis, J. A. Rogers, R. G. Nuzzo, *Small* **2005**, *1*, 1164.
[8] Y. Zhang, Q. Sun, B. Leung, J. Simon, M. L. Lee, J. Han, *Nanotechnology* **2011**, *22*, 045603.
[9] Y. Zhang, B. Leung, J. Han, *Appl. Phys. Lett.* **2012**, *100*, 181908.
[10] K. Chung, C.-H. Lee, G.-C. Yi, *Science* **2010**, *330*, 655.
[11] Y. Kobayashi, K. Kumakura, T. Akasaka, T. Makimoto, *Nature* **2012**, *484*, 223.
[12] D. Chen, H. Xiao, J. Han, *J. Appl. Phys.* **2012**, *112*, 064303.
[13] D. Chen, J. Han, *Appl. Phys. Lett.* **2012**, *101*, 221104.

[14] A. M. Kiefer, D. M. Paskiewicz, A. M. Clausen, W. R. Buchwald, R. A. Soref, M. G. Lagally, *ACS Nano* **2011**, *5*, 1179.
[15] Z. L. Wang, *Adv. Mater.* **2012**, *24*, 4632.
[16] M. M. Roberts, L. J. Klein, D. E. Savage, K. A. Slinker, M. Friesen, G. Celler, M. A. Eriksson, M. G. Lagally, *Nat. Mater.* **2006**, *5*, 388.
[17] S. Keller, Y.-F. Wu, G. Parish, N. Ziang, J. J. Xu, B. P. Keller, S. P. DenBaars, U. K. Mishra, *IEEE Trans. Electron Devices* **2001**, *48*, 552.
[18] K. Kumakura, T. Makimoto, N. Kobayashi, T. Hashizume, T. Fukui, H. Hasegawa, *Appl. Phys. Lett.* **2005**, *86*, 052105.
[19] H. M. Ng, D. Doppalapudi, T. D. Moustakas, N. G. Weimann, L. F. Eastman, *Appl. Phys. Lett.* **1998**, *73*, 821.
[20] H. Zhou, J.-H. Seo, D. M. Paskiewicz, Y. Zhu, G. K. Celler, P. M. Voyles, W. Zhou, M. G. Lagally, Z. Ma, *Sci. Rep.* **2013**, *3*.
[21] M. Kočan, A. Rizzi, H. Lüth, S. Keller, U. k. Mishra, *Phys. Status Solidi B* **2002**, *234*, 773.
[22] R. Calarco, M. Marso, T. Richter, A. I. Aykanat, R. Meijers, A. v. d. Hart, T. Stoica, H. Lüth, *Nano Lett.* **2005**, *5*, 981.
[23] E. Muñoz, E. Monroy, J. A. Garrido, I. Izpura, F. J. Sánchez, M. A. Sánchez-García, E. Calleja, B. Beaumont, P. Gibart, *Appl. Phys. Lett.* **1997**, *71*, 870.
[24] H.-Y. Chen, R.-S. Chen, N. K. Rajan, F.-C. Chang, L.-C. Chen, K.-H. Chen, Y.-J. Yang, M. A. Reed, *Phys. Rev. B* **2011**, *84*, 205443.
[25] F. González-Posada, R. Songmuang, M. Den Hertog, E. Monroy, *Nano Lett.* **2012**, *12*, 172.
[26] R. S. Chen, C. Y. Lu, K. H. Chen, L. C. Chen, *Appl. Phys. Lett.* **2009**, *95*, 233119.
[27] H. Kim, J.-H. Ryou, R. D. Dupuis, S.-N. Lee, Y. Park, J.-W. Jeon, T.-Y. Seong, *Appl. Phys. Lett.* **2008**, *93*, 192106.
[28] D. S. Lee, J. W. Chung, H. Wang, X. Gao, S. Guo, P. Fay, T. Palacios, *IEEE Electron Device Lett.* **2011**, *32*, 755.
[29] W. Huang, T. Khan, T. P. Chow, *IEEE Electron Device Lett.* **2006**, *27*, 796.
[30] Y. Sun, J. A. Rogers, *Adv. Mater.* **2007**, *19*, 1897.
[31] L. M. Mansfield, K. A. Bertness, P. T. Blanchard, T. E. Harvey, A. W. Sanders, N. A. Sanford, *J. Electron. Mater.* **2009**, *38*, 495.
[32] P. T. Blanchard, K. A. Bertness, T. E. Harvey, A. W. Sanders, N. A. Sanford, S. M. George, D. Seghete, *IEEE Trans. Nanotechnol.* **2012**, *11*, 479.
[33] I. Daumiller, D. Theron, C. Gaquiere, A. Vescan, R. Dietrich, A. Wieszt, H. Leier, R. Vetury, U. K. Mishra, I. P. Smorchkova, S. Keller, C. Nguyen, E. Kohn, *IEEE Electron Device Lett.* **2001**, *22*, 62.